INTERNATIONAL JOURNAL OF OPTIMIZATION IN CIVIL ENGINEERING
Int. J. Optim. Civil Eng., 2012; 2(2):247-271

IMPOSITION OF ESSENTIAL BOUNDARY CONDITIONS IN ISOGEOMETRIC ANALYSIS USING THE LAGRANGE MULTIPLIER METHOD

S. Shojaee[*, †], E. Izadpenah and A. Haeri
Department of Civil Engineering, Shahid Bahonar University, Kerman, Iran

ABSTRACT

NURBS-based isogeometric analysis (IGA) has currently been applied as a new numerical method in a considerable range of engineering problems. Due to non-interpolatory characteristic of NURBS basis functions, the properties of Kronecker Delta are not satisfied in IGA, and as a consequence, the imposition of essential boundary condition needs special treatment. The main contribution of this study is to use the well-known Lagrange multiplier method to impose essential boundary conditions for improving the accuracy of the isogeometric solution. Unlike the direct and transformation methods which are based on separation of control points, this method is capable of modeling incomplete Dirichlet boundaries. The solution accuracy and convergence rates of proposed method are compared with direct and transformation methods through various numerical examples.

Received: 21 February 2012; Accepted: 4 June 2012

KEY WORDS: isogeometric analysis; NURBS, essential boundary conditions; lagrange multiplier

1. INTRODUCTION

Isogeometric analysis (IGA) is introduced as a powerful numerical method by Hughes et al. [1]. This method is similar with finite element method (FEM) but takes some inspiration from Computer Aided Design (CAD) tools. IGA is currently of great interest in various engineering problems (e.g. [2-12]). This method is based on Non-Uniform Rational B-splines (NURBS) which

[*]Corresponding author: S. Shojaee, Department of Civil Engineering, Shahid Bahonar University, Kerman, Iran
[†]E-mail address: saeed.shojaee@uk.ac.ir (S. Shojaee)

are used in accurate geometrical modeling and approximation of solution space. Simple and systematic refinement strategies, exact representation of common engineering shapes, robustness and superior accuracy can be achieved in IGA in comparison with the conventional FEM.

In spite of these advantages, the IGA method suffers from some deficiencies. One of the most significant drawbacks arises from imposition of essential boundary conditions. Due to the non-interpolating nature of NURBS basis functions, the properties of Kronecker Delta are not satisfied, and as a consequence, the imposition of essential boundary conditions needs special treatment. In considering this, several methods have been proposed for imposing essential boundary conditions in IGA. This issue for NURBS-based isogeometric analysis was first discussed by Hughes et al. [1]. In their work the essential boundary conditions were imposed to the control variables by evaluating the function of boundary condition at the spatial locations of the control points. In present study this approach is referred as Direct Method (DM) as mentioned by Wang and Xuan [13]. This method is efficient for homogenous boundary conditions but it is not reliable in non-homogenous boundary conditions. In addition, when the position of boundary control points is not located on the desired boundary, it even is not reasonable to enforce the given boundary values to the corresponding boundary control variables [13]. Therefore, the enhancement of essential boundary conditions in IGA needs to be researched more thoroughly [1]. Wang and Xuan [13] have proposed an improved method for imposition of essential boundary conditions in IGA. Here this method is referred as TM (Transformation Method) which is based on concepts of the mixed transformation method that was originated by Chen and Wang [14]. This method produces more accurate results and convergence rates in comparison with DM [13]. However it should be considered that selected boundary points can result in singular transformation matrix. This drawback is more significant when there are many active control points on desired boundary and more careful selection procedure is needed. As mentioned by Wang and Xuan [13], a set of boundary interpolation points can be selected to construct the appropriate transformation matrix.

TM and DM are based on separation of control points into boundary and interior ones. This separation can complicate the imposition of essential boundary conditions in problems with incomplete Dirichlet boundaries. Without loss of generality consider following beam which is modeled by $x=\{0 \quad 0 \quad 0 \quad 1 \quad 1 \quad 1\}$ and $h=\{0 \quad 0 \quad 0 \quad 1 \quad 1 \quad 1\}$ knot vectors. As shown in Figure 1 the Dirichlet boundary is defined on left side of beam with a length of L_D. Corresponding NURBS basis functions to control points 1, 2 and 3 are boundary functions as they are active on Γ_D, therefore in DM and TM control variable values corresponding to these control points will be equal to zero. Even more, for interior control points (4-9) the corresponding NURBS basis functions are inactive on Γ_D, so the whole length of left side of the beam, L, is considered constrained. As a result, DM and TM are not efficient methods for modeling these types of Dirichlet boundaries.

In this paper, Lagrange multiplier (LM) method is proposed for improving the imposition of essential boundary conditions in IGA. In mathematics, this method is used for transforming a constrained optimization problem to an unconstrained problem. This method has been widely used in various approaches because of its straightforward implementation (e.g. in traditional FEM [15-18], extended FEM [19-20], meshfree methods [21-24]). Unlike DM and TM, this method is not based on separation of control points and is capable of modeling

incomplete Dirichlet boundaries (e.g. Figure 1).

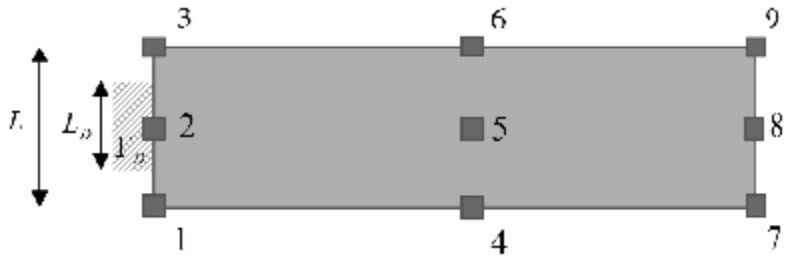

Figure 1. Incompelete Dirichlet boundary on a beam

This paper is organized as follows. First, the NURBS-based IGA is briefly reviewed. Then, formulation of enhanced IGA with proposed method is presented. Finally, results of the numerical simulations of several problems are discussed and the efficiency of the proposed approach is confirmed by comparing with available reference results.

2. ISOGEOMETRIC ANALYSIS BASED ON THE NURBS BASIS FUNCTIONS

2.1. Overview of the isogeometric analysis

The traditional finite element formulations are based on interpolation schemes with Lagrange, Legendre or Hermit polynomials to approximate the geometry, the physical field and its derivatives. This approach often requires a substantial simplification of the geometry, particularly in the case of curved boundaries of the analysis domain. Generally, adaptive refinement of the discretized domain is applied to better approximate the boundary and to achieve sufficient convergence.

The concept of IGA introduced by Hughes et.al [1] is based on applying the NURBS basis functions in accurate modeling of geometry and approximation of solution space.

The NURBS basis functions are weighted functions which originate from B-spline interpolation. The B-spline functions are defined on a knot vector. A knot vector is a suite of non-descending real numbers, which is presented by,

$$x = \left\{x_1, x_2, ..., x_{n+p+1}\right\} \tag{1}$$

where x_i is the ith knot value, n and p are respectively the number and the order of basis functions defined on knot vector. The half open interval, $[x_i, x_{i+1})$, is called knot interval. If $x_i = x_{i+1}$ then the length of knot interval is equal to zero. If x_1 and x_{n+p+1} are repeated p+1 times in a knot vector, the resulting knot vector is called open knot vector. The first order B-spline is defined on knot vector by,

$$N_{i,0}(x) = \begin{cases} 1 & \text{if } x_i \le x < x_{i+1} \\ 0 & \text{otherwise} \end{cases} \tag{2}$$

And higher order basis functions are recursively defined by,

$$N_{i,j}(x)=\frac{x-x_i}{x_{i+j}-x_i}N_{i,j-1}(x)+\frac{x_{i+j+1}-x}{x_{i+j+1}-x_{i+1}}N_{i+1,j-1}(x)$$
$$j=1,2....,p \qquad (3)$$
$$i=1,2,.....,n+p+1-j$$

In which $N_{i,j}$ is the ith basis function with a j order. The first order derivative of B-spline is,

$$\frac{d}{dx}N_{i,j}(x)=\frac{j}{x_{i+j}-x_i}N_{i,j-1}(x)-\frac{j}{x_{i+j+1}-x_{i+1}}N_{i+1,j-1}(x) \qquad (4)$$

The third order B-spline functions which are obtained by knot vector of $x=\{0\ 0\ 0\ 0.5\ 0.5\ 1\ 1\ 1\}$ are shown in Figure 2.

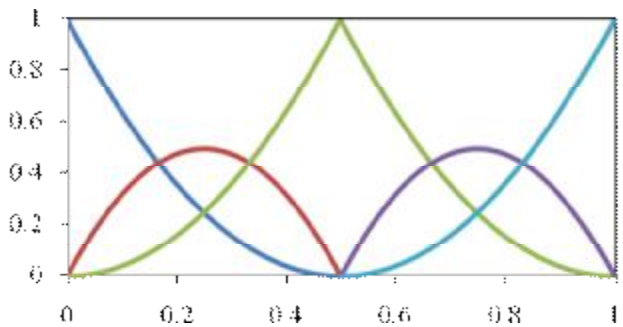

Figure 2. Quadratic B-splines functions

The NURBS basis functions are made from B-spline functions by following equation,

$$R_{i,p}(x)=\frac{N_{i,p}w_i}{W(x)} \qquad (5)$$

In which w_i is the weight corresponding to ith control point and $W(x)$ is weight function,

$$W(x)=\sum_{i=1}^{n}N_{i,p}w_i \qquad (6)$$

The bivariate NURBS functions on $x-h$ knot surface are defined by:

$$R_{i,j}^{p,q}(x,h)=\frac{N_{i,p}(x)M_{j,q}(h)w_{i,j}}{W(x,h)} \qquad (7)$$

$$i = 1, 2...., n$$
$$j = 1, 2..., m$$

In which $M_{j,q}$ and $N_{i,p}(x)$ are respectively the *i*th *p*-order and *j*th *q*-order functions on x and h knot vectors. $w_{i,j}$ is the weight corresponding to *ij* control point and $W(x,h)$ is the bivariate weight function which is given by,

$$W(x,h) = \sum_{i=1}^{n} \sum_{j=1}^{m} N_{i,p}(x) M_{j,q}(h) w_{i,j} \tag{8}$$

2.2. Two-dimensional stress analysis

Isogeometric analysis of stress field with NURBS discretizations is a well studied topic, with applications in applied mechanics. The model problem which we consider here is the differential equation of stress field for isotropic material with elastic behavior,

$$\nabla . s + f_b = 0 \qquad in\ \Omega \tag{9a}$$

$$s . n = f_t \qquad on\ \Gamma_N \tag{9b}$$

$$s . n = 0 \qquad on\ \Gamma_F \tag{9c}$$

$$u = \bar{u} \qquad on\ \Gamma_D \tag{9d}$$

where s is stress tensor, f_b and f_t are body and surface force vectors respectively, n is normal vector on boundary, and $\bar{u}$ is known displacement on Γ_D boundary. The boundary is divided into three parts, Γ_D (Dirichlet boundary), Γ_N (Neumann boundary), and Γ_F (free boundary). The following equations should be satisfied,

$$\Gamma_D \cup \Gamma_N \cup \Gamma_F = d\ \Omega \tag{10a}$$

$$\Gamma_D \cap \Gamma_N \cap \Gamma_F = \varnothing \tag{10b}$$

Dirichlet and Neumann boundaries are shown in Figure 3.

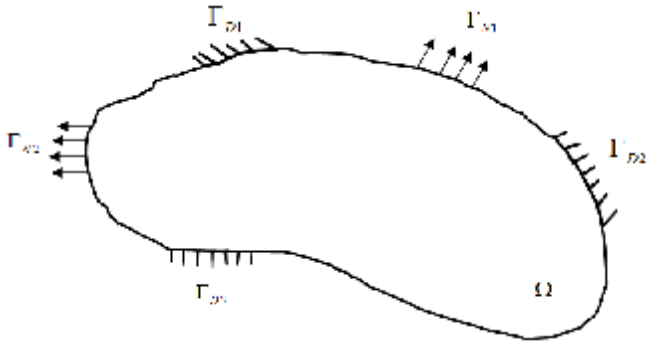

Figure 3. Neumann and Dirichlet boundaries

It can be shown that the corresponding functional of stress field is the potential energy of system,

$$p = \frac{1}{2}\int_{\Omega} e^T s \, d\Omega - \int_{\Omega} u^T f_b d\Omega - \int_{\Gamma_N} u^T f_t d\Gamma \tag{11}$$

The first term in Eq. (11) is the conserved strain energy in the system; the second and third terms are work of body and surface forces respectively.

2.3. General class of problems

The development of isogeometric analysis was applied to a very general class of problems, and various models have been considered in literature [25]. In this subsection, the formulation of scalar potential problem is considered. Let us denote the domain solution by Ω with boundary Γ, the potential equation within the domain Ω is defined as,

$$\begin{cases} \Delta u + s = 0 & in\ \Omega \\ n.\nabla u = t & on\ \Gamma_N \\ u = g & on\ \Gamma_D \end{cases} \tag{12}$$

where Δ denotes the Laplacian operator and *s* is the source term, *t* and *g* denote the Neumann and Dirichlet boundaries conditions respectively. The functional corresponding to Eq. (12) is given by,

$$p(u) = \frac{1}{2}\int_{\Omega} \nabla u.\nabla u \, d\Omega - \int_{\Omega} u s \, d\Omega - \int_{\Gamma_N} ut \, d\Gamma \tag{13}$$

where ∇ denotes the gradient operator.

2.4. Isogeometric formulation based on the NURBS basis functions

Here, the application of NURBS-based isogeometric analysis is considered to formulate 2D stress analysis problem and can be generalized to other problems. In isogeometric approach,

the discretization is based on NURBS. Hence, the geometry and solution field are approximated as,

$$x(x,h) = RP \qquad x,h \in \Omega_{patch} \tag{14}$$

$$u^h(x,h) = Rd \qquad x,h \in \Omega_{patch} \tag{15}$$

where $\Omega_{patch} = \left\{(x,h) \middle| x \in \left[x_1, x_{n+p+1}\right], h \in \left[h_1, h_{m+q+1}\right]\right\}$. The matrix-form of $R_{i,j}$ and $P_{i,j}$ can be changed into vector-form by mapping from i, j subscripts to k by,

$$k = i + (j-1)n, \qquad \text{with } k = 1, 2, ..., n.m = N \tag{16}$$

So, the control points are defined as:

$$P = \left\{P_{1x} \quad P_{1y} \quad \mathbf{L} \quad \mathbf{L} \quad P_{Nx} \quad P_{Ny}\right\}^T \tag{17}$$

The values of solution field at the control points, also called control variables, in the present IGA formulation are displacements and can be arranged similar to the control points in a vector-form:

$$d = \left\{d_{1x} \quad d_{1y} \quad \mathbf{L} \quad \mathbf{L} \quad d_{Nx} \quad d_{Ny}\right\}^T \tag{18}$$

The matrix R is obtained from NURBS basis functions,

$$R = \begin{bmatrix} R_1 & 0 & R_2 & 0 & \mathbf{L} & \mathbf{L} & R_N & 0 \\ 0 & R_1 & 0 & R_2 & \mathbf{L} & \mathbf{L} & 0 & R_N \end{bmatrix} \tag{19}$$

Next, the stiffness matrix for a single patch is computed as,

$$k_{patch} = t \iint_{\hat{\Omega}} B^T(x,h) D B(x,h) \left|J\right| d\hat{\Omega} \tag{20}$$

where t is the plate thickness, $\hat{\Omega}$ is the parametric space and $B(x,h)$ is the strain-displacement matrix, given as:

$$B(x,h) = \begin{bmatrix} \dfrac{\partial}{\partial x} & 0 \\ 0 & \dfrac{\partial}{\partial y} \\ \dfrac{\partial}{\partial y} & \dfrac{\partial}{\partial x} \end{bmatrix} R \tag{21}$$

Where

$$\begin{pmatrix} \dfrac{\partial R}{\partial x} \\ \dfrac{\partial R}{\partial y} \end{pmatrix} = J^{-1} \begin{pmatrix} \dfrac{\partial R}{\partial x} \\ \dfrac{\partial R}{\partial h} \end{pmatrix} \tag{22}$$

and J is the Jacobian matrix which maps the parametric space to the physical space and is defined as:

$$J = \begin{bmatrix} \dfrac{\partial x}{\partial x} & \dfrac{\partial y}{\partial x} \\ \dfrac{\partial x}{\partial h} & \dfrac{\partial y}{\partial h} \end{bmatrix} \tag{23}$$

D is the elastic material property matrix for plane stress:

$$D = \frac{E}{1-n^2} \begin{bmatrix} 1 & n & 0 \\ n & 1 & 0 \\ 0 & 0 & \dfrac{1-n}{2} \end{bmatrix} \tag{24}$$

E ,n are Young's modulus and Poisson's ratio, respectively.

The force vector on a single patch in the presence of body forces f_b and traction forces f_t is obtained as:

$$F = \iint_{\Omega} R^T f_b |J| \, d\Omega + \int_{\Gamma_N} R_b^T f_t |J_b| \, d\Gamma \tag{25}$$

Where Ω and Γ are the domain and traction boundary in the parametric space, R_b is the NURBS basis function evaluated on the traction boundary and J_b is the Jacobian that maps the traction boundary into a part of physical space boundary. The control variables can then be solved by the following discretized equilibrium equation,

$$Kd = F \tag{26}$$

The solution field at each point of the physical space can be approximated by Eq. (15). For numerical integration, the standard Gauss-quadrature is used over each element (knot span). The number of quadrature points depends on the NURBS order. The details of spaces, mapping and integration in isogeometric analysis are shown in Figure 4. Note that the physical mesh is only an image of knot spans on the physical space.

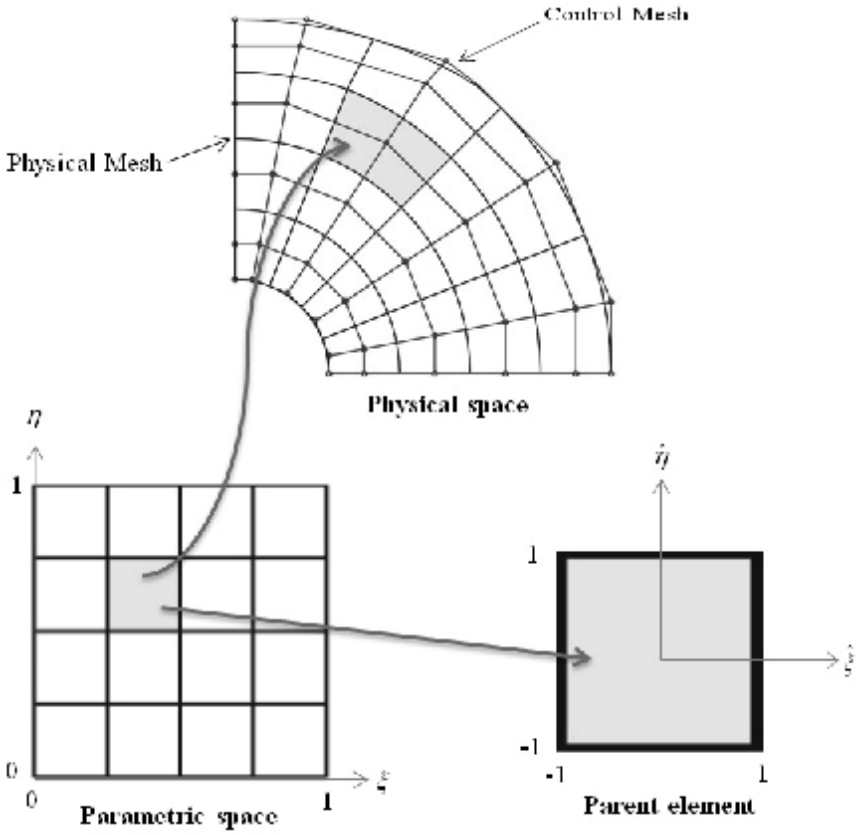

Figure 4. Physical space Ω is mapped into the parametric space $\tilde{\Omega}$ using NURBS basis functions (Eq. 14). For numerical integration in the parametric space, each knot span (element) is mapped to the parent element, where the integration is performed on

2.5. h-Refinement or knot insertion

For the convergence study, *h*-refinement strategy has been applied to the initial geometry of model. In each refinement step, knots are added to the knot spans. Knot insertion is a procedure that arbitrary new knots are added to a knot vector without any change in the shape of the B-spline curve. If there are $m = n + p + 1$ knots in the knot vector of the B-spline curve, where n is the number of control points and p is the order of B-spline curve, by adding a new knot, a new control point must be added. Also, some current control points must be redefined.

Consider a knot vector $x = \{x_1, x_2, ..., x_{m=n+p+1}\}$ with n control points $P_1, P_2, ..., P_n$ and the order of p. Let $\hat{x} \in [x_k, x_{k+1}]$ be a desired new knot. The knot insertion procedure has the following 3 steps [26]:

1. Find k such that $\hat{x}$ belongs to $[x_k, x_{k+1}]$.
2. Find $p+1$ control points $P_{k-p}, P_{k-p+1}, ..., P_k$.

3. Compute p new control points Q_i from the above $p+1$ control points by using Eq. (27).

$$Q_i = (1-a_i)P_{i-1} + a_i P_i \tag{27}$$

where a_i is obtained from,

$$a_i = \frac{\hat{x} - x_i}{x_{i+p} - x_i} \quad \text{for} \quad k-p+1 \le i \le k \tag{28}$$

By performing the above procedure, the new knot vector and control points are obtained as,

$$\begin{gathered} \left\{x_1, x_2, ..., x_k, \hat{x}, x_{k+1}, ..., x_m\right\} \\ \left\{P_1, P_2, ..., P_{k-p}, Q_{k-p+1}, Q_{k-p+2}, ..., Q_k, P_k, P_{k+1}, ..., P_n\right\} \end{gathered} \tag{29}$$

Now, this knot insertion algorithm is extended to a NURBS curve. For this purpose, a given NURBS curve in d-dimensional space is converted into a B-spline curve in (d+1)-dimensional space, then by applying the knot insertion algorithm in this B-spline curve, the new control points are obtained. These new control points should then be projected to d-dimensional space to obtain the new control points of the NURBS curve. Consider control points $P_i = (x_i, y_i)$ with corresponding weights of w_i, by converting these control points to 3-dimensional space, $P_i^w = (w_i x_i, w_i y_i, w_i)$, the new control points are then computed from Eq. (27),

$$Q_i^w = (1-a_i)P_{i-1}^w + a_i P_i^w \tag{30}$$

The location of control points in 2D are obtained by the following projection technique:

$$Q_i = \frac{(1-a_i)P_{i-1}^w + a_i P_i^w}{(1-a_i)w_{i-1} + a_i w_i} \tag{31}$$

and the weights are:

$$w_{Q_i} = (1-a_i)w_{i-1} + a_i w_i \tag{32}$$

3. IMPOSITION OF ESSENTIAL BOUNDARY CONDITION USING LAGRANGE MULTIPLIER METHOD

In mathematical optimization, the method of Lagrange multiplier provides a strategy for finding the maximum and minimum of a function or functional subject to constraints. An element called the Lagrange multiplier (λ) makes a new term with constraints which can be either added or subtracted with objective function and results in the Lagrange function or functional. Then the optimum solutions for objective function or functional is obtained by finding stationary points of them (where the variations of Lagrange function or functional are

zero). In this study, the Lagrange multiplier method is employed as a scheme for treatment of essential boundary conditions.

Considering the problem of minimizing the total potential energy functional of stress field problem given by,

$$\begin{aligned}
&\text{minimize}: \quad p = \frac{1}{2} t \int_{\Omega} e^T s \, d\Omega - t \int_{\Omega} u^T f_b d\Omega - \int_{\Gamma_N} u^T f_t d\Gamma \\
&\text{subject to}: \\
&g_1 = u - \bar{u}_1 \qquad on\ \Gamma_{D1} \\
&g_2 = u - \bar{u}_2 \qquad on\ \Gamma_{D2} \\
&. \\
&. \\
&. \\
&g_m = u - \bar{u}_m \qquad on\ \Gamma_{Dm}
\end{aligned} \tag{33}$$

Where $u = \{u_x, u_y\}^T$ is the degrees of freedom vector of system, $\bar{u}_i = \{\bar{u}_{xi}, \bar{u}_{yi}\}^T$ is the known value of displacement on Γ_{Di} boundary, t is the thickness of object and m is the number of Dirichlet boundaries. For the inclusion of the constraints into the variational problem, using Lagrange multiplier method, instead of seeking the minimum of p subjected to constraints, the Lagrange method seeks the stationary points that satisfies Eq. (34),

$$\text{minimize}: \quad p^* = \frac{1}{2} t \int_{\Omega} e^T s \, d\Omega - t \int_{\Omega} u^T f_b d\Omega - \int_{\Gamma_N} u^T f_t d\Gamma - \sum_{i=1}^{m} \int_{\Gamma_{Di}} l_i (u - \bar{u}_i) d\Gamma \tag{34}$$

where l_i is the Lagrange multiplier vector, corresponding to Γ_{Di} and is defined by,

$$l_i = \begin{Bmatrix} l_{ix} \\ l_{iy} \end{Bmatrix} \tag{35}$$

Now with approximation of l_i and u, exact solution space will transform to approximate solution space,

$$u \cong u^h = Rd \tag{36}$$

where R and d are defined in Eqs. (18) and (19). Then Lagrange multiplier vector is discretized for obtaining matrix form of problem,

$$l_i = N_i \bar{l}_i \qquad i = 1, 2...., m \tag{37a}$$

$$N_i = \begin{bmatrix} N_1^i & 0 & \mathbf{L} & \mathbf{L} & N_{nl}^i & 0 \\ 0 & N_1^i & \mathbf{L} & \mathbf{L} & 0 & N_{nl}^i \end{bmatrix} \tag{37b}$$

$$\bar{l}_i = \left\{ l_{1x}^i \quad l_{1y}^i \quad ..... \quad l_{nlx}^i \quad l_{nly}^i \right\}^T \tag{37c}$$

where nl is number of Lagrange multipliers. $N_i(l)$ is a single-variable NURBS function given by Eqs. (2) and (3), where l is one of parametric components (x or h).

$N_i(l)$ is defined on following kont vector

$$\bar{l}_i = \left\{ l_1^i, ..., l_1^i, l_2^i, l_3^i, ..., l_{n-1}^i, l_n^i, ..., l_n^i \right\}^T \tag{38}$$

where l_1^i and l_n^i are the coordinates of ith Dirichlet boundary end points in parametric space, which are repeated $\bar{p}$ times. $\bar{p}$ is either p or q depended on direction of Dirichlet boundary in parametric space.

Substituting Eqs. (36) and (37a) into Eq. (34), we have,

$$p^* = \frac{1}{2} t d^T \int_\Omega B^T D B \, d\Omega d - t d^T \int_\Omega R^T f_b \, d\Omega - d^T \int_{\Gamma_N} R^T f_t \, d\Gamma - \sum_{i=1}^{m} \bar{l}_i^T \int_{\Gamma_{Di}} N_i^T (Rd - \bar{u}_i) d\Gamma \tag{39}$$

The required solution of the problem is obtained by setting $\partial p^* / \partial d$ and $\partial p^* / \partial \bar{l}_i$ to zero,

$$t \int_\Omega B^T D B d\Omega d - t \int_\Omega R^T f_b \, d\Omega - \int_{\Gamma_N} R^T f_t \, d\Gamma - \sum_{i=1}^{m} \int_{\Gamma_{Di}} R^T N_i \, d\Gamma \bar{l}_i = 0 \tag{40a}$$

$$\int_{\Gamma_{Di}} N_i^T R \, d\Gamma d = \int_{\Gamma_{Di}} N_i^T \bar{u}_i \, d\Gamma \qquad i = 1, 2, ..., m \tag{40b}$$

Then we obtain the system of algebraic equations,

$$\begin{bmatrix} K & G \\ G^T & 0 \end{bmatrix} \begin{Bmatrix} d \\ \bar{l} \end{Bmatrix} = \begin{Bmatrix} f \\ q \end{Bmatrix} \tag{41}$$

where,

$$K = \int_\Omega B^T D B \, d\Omega \tag{42a}$$

$$G = -\begin{bmatrix} G_1 & \mathbf{L} & \mathbf{L} & G_m \end{bmatrix} \quad , \quad G_i = \int_{\Gamma_{Di}} R^T N_i \, d\Gamma \tag{42b}$$

$$q = -[q_1 \quad \mathbf{L} \quad \mathbf{L} \quad q_m] \qquad , \qquad q_i = \int_{\Gamma_{Di}} N_i^T \bar{u}_i \, d\Gamma \tag{42c}$$

$$f = t\int_{\Omega} R^T f_b \, d\Omega + \int_{\Gamma_N} R^T f_t \, d\Gamma \tag{42d}$$

$$\bar{l} = \left\{ \bar{l}_1 \quad \bar{l}_2 \quad \mathbf{L} \quad \mathbf{L} \quad \bar{l}_m \right\}^T \tag{42e}$$

For imposition of essential boundary conditions in potential equation Eq. (12), the following term is subtracted from Eq. (13),

$$\sum_{i=1}^{m} \int_{\Gamma_{Di}} l_i (u - g_i) d\Gamma \tag{43}$$

The modified functional corresponding to Eq. (12) is,

$$p^*(u) = \frac{1}{2}\int_{\Omega} \nabla u . \nabla u \, d\Omega - \int_{\Omega} u \, s \, d\Omega - \int_{\Gamma_N} ut \, d\Gamma - \sum_{i=1}^{m} \int_{\Gamma_{Di}} l_i (u - g_i) d\Gamma \tag{44}$$

By approximation of u and l and minimizing p^* with respect to d and $\bar{l}$ vectors, the following system of algebric equations is obtained,

$$\begin{bmatrix} K & G \\ G^T & 0 \end{bmatrix} \begin{Bmatrix} d \\ \bar{l} \end{Bmatrix} = \begin{Bmatrix} f \\ q \end{Bmatrix} \tag{45}$$

where,

$$K = \int_{\Omega} \nabla R^T . \nabla R \, d\Omega \tag{46a}$$

$$f = \int_{\Omega} R^T s d\Omega + \int_{\Gamma_N} R^T t \, d\Gamma \tag{46b}$$

Other parameters in Eq. (45) are defined in Eqs. (42b-e). It is also worthwhile to note that the defined parameters in these equations can be modified for single degree of freedom state.

4. NUMERICAL EXAMPLES

The accuracy and robustness of proposed method for imposition of essential boundary conditions are investigated through several numerical examples. For convergence study, the order of NURBS basis function (OF) is set to be 3 in both directions (OF=p=q=3). Numerical

integration within each element is carried out by 9×9 Gauss quadrature rule. The examples are also solved by higher orders (OF=4 and OF=5) to investigate the effect of higher orders on accuracy. Knot insertion procedure is applied in these examples for estimation of errors and convergence study and the L^2-error norms are normalized with respect to their corresponding norms from the analytical solutions. In last example, an incomplete Diritchlet boundary problem is solved with three methods and compared with results obtained from FEM with a fine meshing. The effect of number of Lagrange multipliers (N_l) on error-norm, and running time in all examples are compared for three methods in Section 5.

4.1. Potential equation

Consider the potential problem on a quarter disk domain in Figure 5. The governing equation and boundary conditions are given in Eq. (12). The source term and boundary conditions for this problem are given by,

$$\begin{aligned} & s = 0.02 \\ & u = 0 \quad \text{on} \quad \Gamma_{D1} \quad , \quad u = 37.5 \quad \text{on} \quad \Gamma_{D2} \\ & u = \frac{100^2 - x^2}{200} \quad \text{on} \quad \Gamma_{D3} \quad , \quad u = \frac{100^2 - y^2}{200} \quad \text{on} \quad \Gamma_{D4} \end{aligned} \tag{47}$$

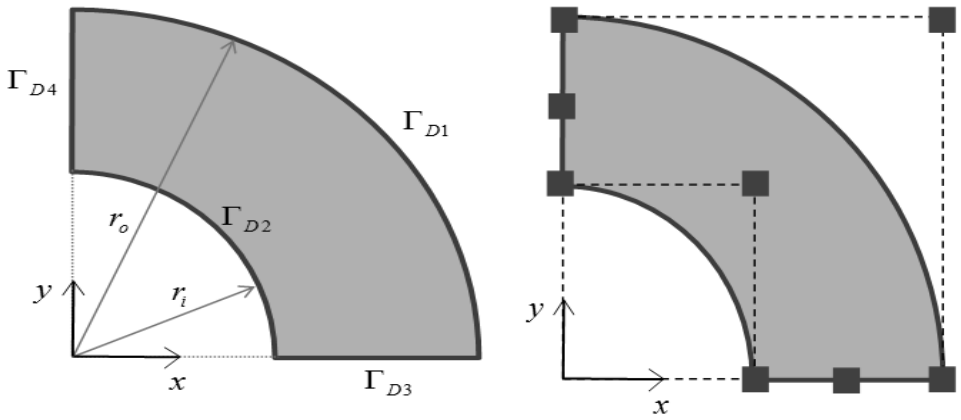

(a) (b)

Figure 5. (a) Quarter disk, r_i=*50cm* and r_o=*100cm*; (b) Position of boundary control points

So, the exact solution is obtained as,

$$u_{(x,y)} = \frac{100^2 - x^2 - y^2}{200} \tag{48}$$

The initial geometry is constructed by tensor product of quadratic NURBS basis functions. The initial parametric space is given by two knot vectors of the form,

$x = \{0\ 0\ 0\ 0.2\ 0.4\ 0.6\ 0.8\ 1\ 1\ 1\}$ and $h = \{0\ 0\ 0\ 0.2\ 0.4\ 0.6\ 0.8\ 1\ 1\ 1\}$.

Using h refinement strategy, meshes with 25, 100 and 225 elements are considered for the convergence study (Figure 6).

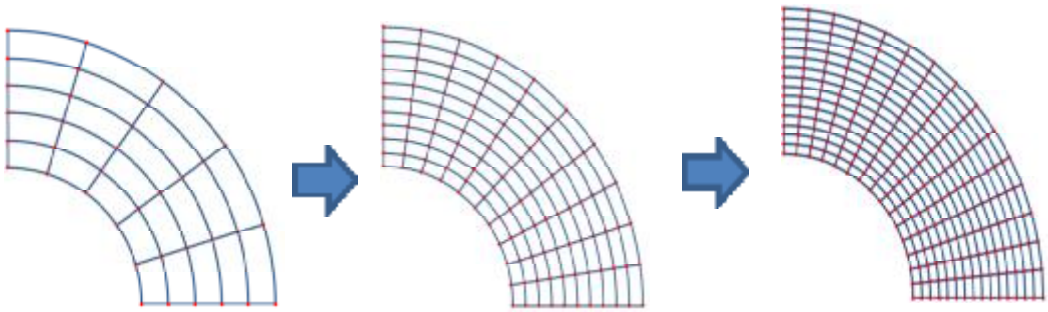

Figure 6. Improvement of meshing by knot insertion procedure in example 2

The results obtained from three methods are compared in Figure 7. Since the control points are not located on Γ_{D1} and Γ_{D2} boundaries (Figure 5b), the DM has the least accuracy in comparison with two other methods, moreover the difference between error norms of DM and two other methods are remarkable. On the other hand, LM and TM have fairly the same L^2-error norm which is almost constant in meshing refinement procedure. This implies that LM and TM have converged in coarse meshing. These observations verify that LM and TM are more efficient than DM in the problems with curved boundaries, where the position of control points is not located on Dirichlet boundaries.

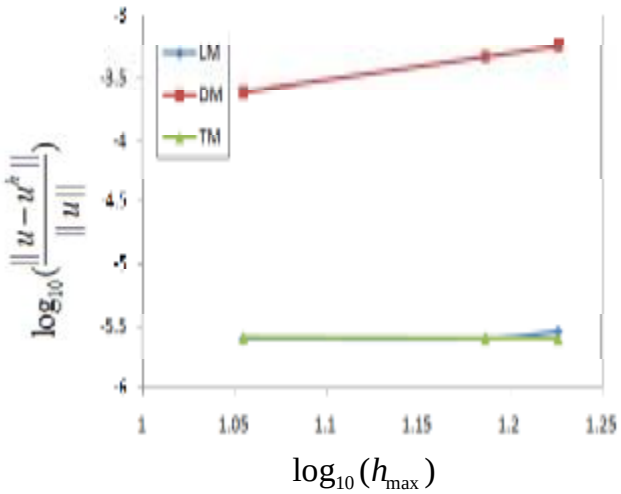

Figure 7. L^2-error norm for potential equation

4.2. Cantilever beam

Consider the cantilever beam problem which is solved by Wang and Xuan [13] as an example for demonstration of TM (Figure 8):

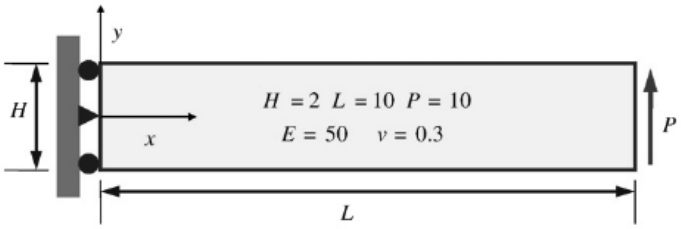

Figure 8. Cantilever beam problem

The analytical solution of this problem for displacement in *y* direction is [27],

$$u_y(x,y)=\frac{p}{6\bar{E}I}\left[(3L-x)x^2+3\bar{n}y^2(L-x)+(4+5\bar{n})\frac{H^2x}{4}\right]$$

$$\begin{cases}\bar{E}=\dfrac{E}{1-n^2}\quad,\quad \bar{n}=\dfrac{n}{1-n} & \text{plane strain}\\ \bar{E}=E\qquad,\quad \bar{n}=n & \text{plane stress}\end{cases} \tag{49}$$

In this example plane stress condition is adopted, and knot vectors used for initial meshing are same as example 1. It is observed that DM still has the highest error among three methods (Figure 9). LM has the best convergence rate in meshing refinement procedure, while the TM results are close to LM in fine meshing.

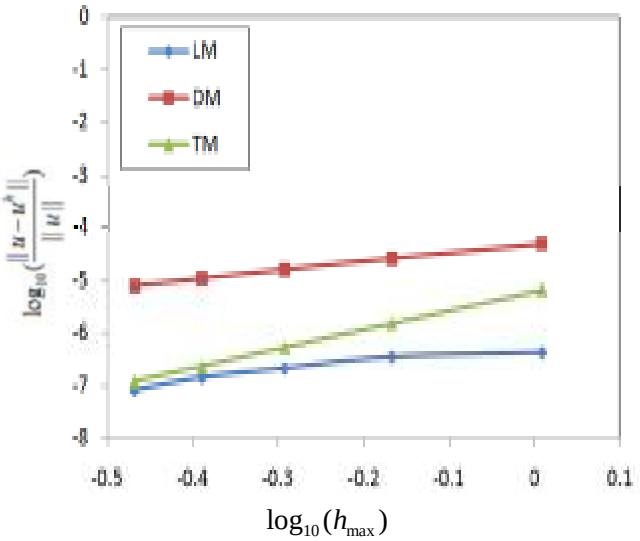

Figure 9. L^2-error norm for cantilever beam

4.3. An infinite plate with a centeral circular hole

In this example, an infinite plate with a circular hole in center under *x*-direction traction T_x is considered, as depicted in Figure 10(a). The analytical solution for displacement in x and y

direction, given in [27], is as follows,

$$u_x(r,q)=\frac{T_x a}{8m}\left\{\frac{r}{a}(k+1)c\,\mathrm{os}q+2\frac{a}{r}((k+1)\cos q+\cos 3q)-2\frac{a^3}{r^3}\cos 3q\right\} \tag{50a}$$

$$u_y(r,q)=\frac{T_x a}{8m}\left\{\frac{r}{a}(k-3)\sin q+2\frac{a}{r}((1-k)\sin q+\sin 3q)-2\frac{a^3}{r^3}\sin 3q\right\} \tag{50b}$$

where m is the shear modules of material and k is given by,

$$k=\begin{cases}3-4n & (plane\ strain)\\ \dfrac{3-n}{1+n} & (plane\ stress)\end{cases} \tag{51}$$

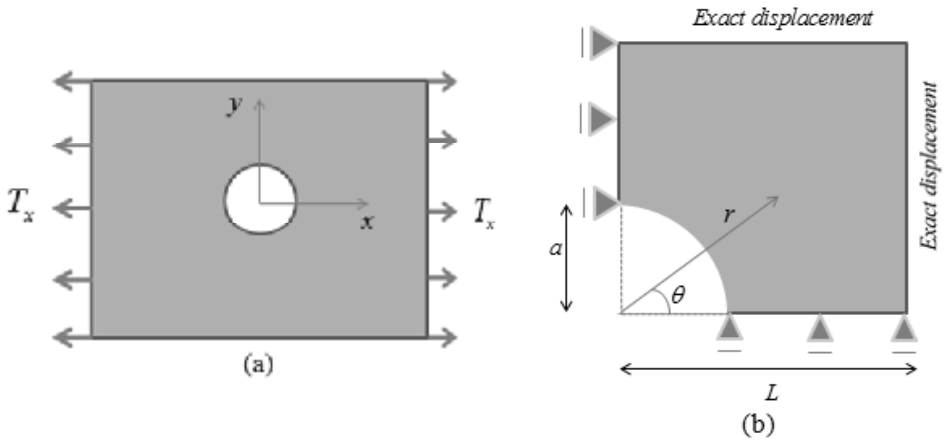

Figure 10. (a) Infinite plate with a circular hole; (b) Numerical model

Due to the symmetry, only one quarter of the domain is considered for numerical simulation. This model is subjected to the essential boundary condition computed from the exact solution. This problem is solved in the plane stress state and the following parameters are considered in the analysis, radius of the circular hole $R=1$, plate width $L=4$, x-direction traction $T_x=10$, modulus of elasticity $E=10^5$ and Poisson's ratio $n=0.3$. Meshes with 100, 400 and 1600 elements are considered for the convergence study (see Figure 11). The L^2 error norms are plotted in Figure 12, which show that good convergence rates is obtained for the Lagrange multiplier and transformation methods. DM is conveging with a lower convergence rate.

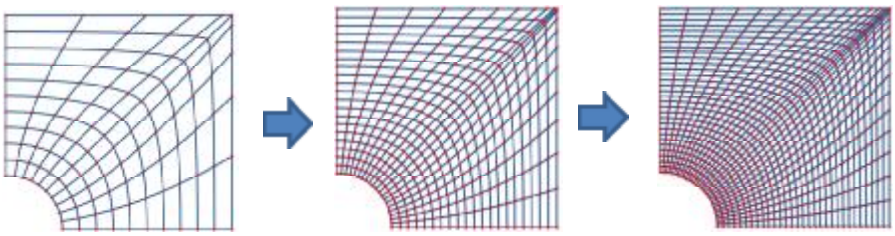

Figure 11. Mesh refinment for a quarter of symmetric infinte plate

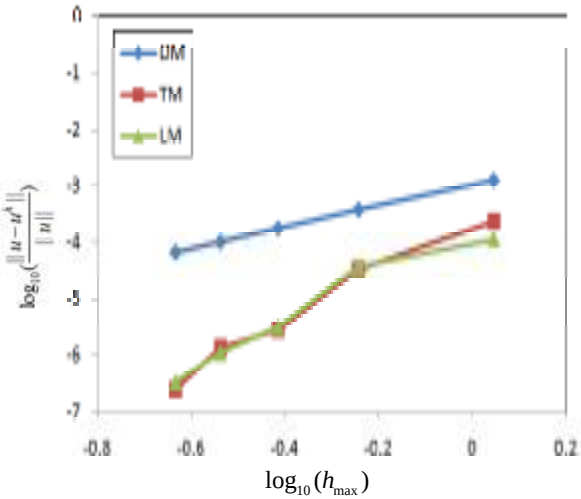

Figure 12. L^2-error norm for infinite plate

Effect of *OF* on error is depicted for 10x10 and 30x30 meshing in Figure 13. Order variation has no significant effects on accuracy of DM. But in TM and LM the error-norm is decreased in higher orders. However in both meshing LM is more accurate than TM.

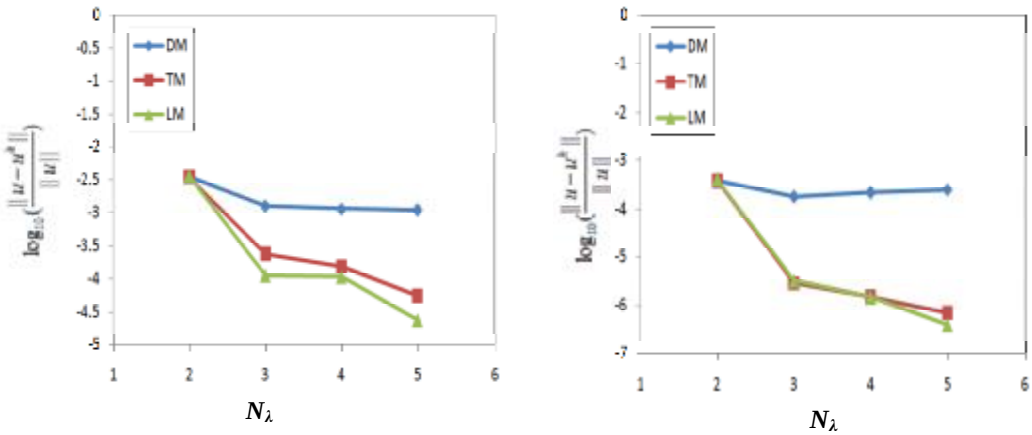

Figure 13. effects of *OF* on L^2-error norm for infinite plate problem (a) 10x10 meshing (b) 30x30 meshing

4.4. Steady-state thermal transfer within hollow disk

In this example, we consider steady-state thermal transfer within hollow disk domain. The thermal conductivity is assumed to be constant unity. The governing equation is then similar to the potential problem in the second example. The geometry of the problem is defined in Figure 14. The exact temperature field in the hollow disk is given as,

$$u(\mathbf{x}) = x^3 + y^4 \tag{52}$$

Using this exact solution, the prescribed temperature field is imposed on the inner and outer boundaries of the hollow disk. The thermal source term can also be derived according to the exact temperature field.

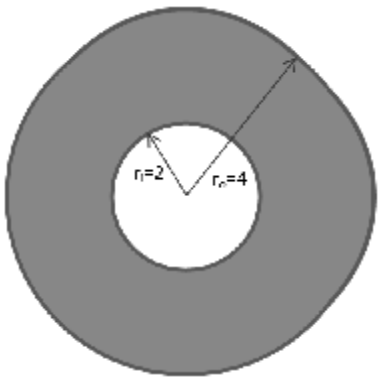

Figure 14. Steady-state heat transfer within hollow disk

To verify the present approach, the results are compared with those obtained using TM. It should be noted that in this problem, unlike previous examples, the boundary control points do not lay on the physical problem boundary. For modeling the initial geometry, quadratic NURBS basis functions in both directions are employed. The initial knot vectors for this problem are, $x = \{0,0,0,0.25,0.25,0.5,0.5,0.75,0.75,1,1,1\}$, $h = \{0,0,0,1,1,1\}$. For one, two and three h-refinements of the initial geometry, physical meshes with 16, 64 and 256 elements are obtained (see Figure 15). The L^2 error norm predicted by the present method, the direct approach and the transformation method are shown in Figure 16. Again, the present approach has provided the least level of errors and the optimal convergence rate in comparison with the other techniques.

Figure 15. Mesh refinement for hollow disk

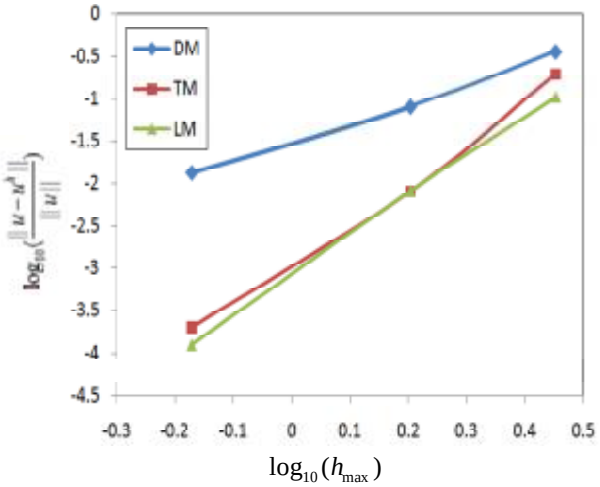

Figure 16. L^2-error norm for hollow disk example

4.5. Incomplete dirichlet boundary

In the last numerical example the accuracy of DM, TM and LM is investigated in problems with incomplete Dirithlet boundaries. Consider the cantilever beam in example 4.3, which is incompletely restrained at the left site as shown in Figure 17. The beam is subjected to a uniform distributed load (w=10 w=10) and the geometrical and mechanical properties are same as example 4.2. Since the exact solution for this problem is not available, the results of three methods are compared with results obtained from finite element method analysis, with a fine meshing consisting of 25000 elements. The adapted element in FEM analysis is composed of four nodes and each node has two degrees of freedom (Figure 18).

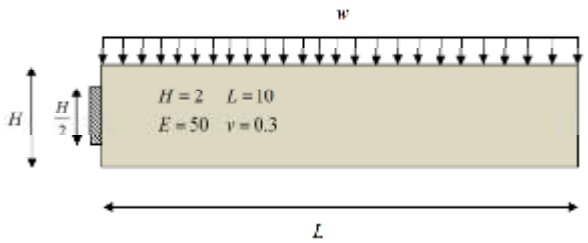

Figure 17. Incomplete Dirichlet boundary problem

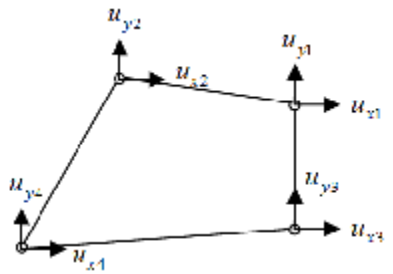

Figure 18. Q4 element

Since the boundary condition of problem is homogenous, so DM and TM have the same accuracy. For convergence study the meshing is refined by 20x20, 24x24, 28x28, 32x32, 36x36 and 40x40 elements. The convergenc rate is depicted for three methods in Figure 19.

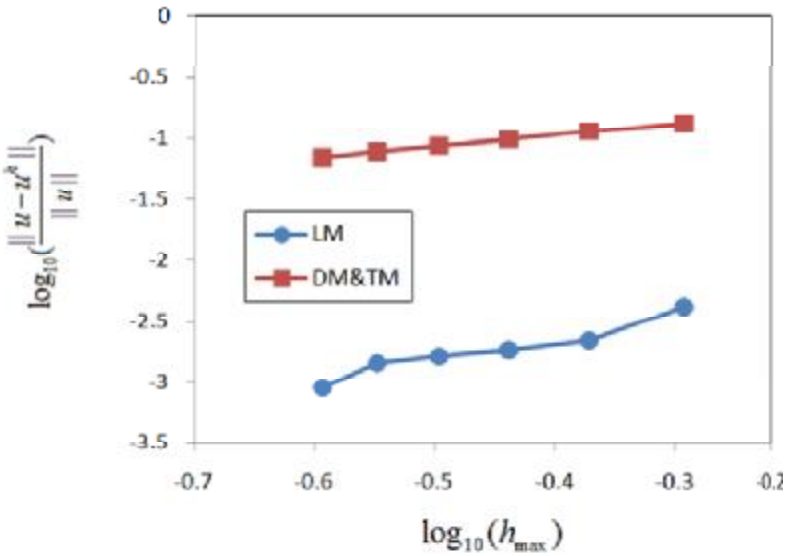

Figure 19. L^2-error norm for incomplete Dirichlet boundary problem

LM has considerably more accuracy than two other methods. As shown in Figure 19, the convergence rate of DM and TM is too low that in very fine meshing the error-norm of these methods still has a noticeable difference with LM. By increasing the number of elements, LM shows more accuracy and its convergence rate is growing. This example implies that LM is more efficient than DM and TM (which are based on separation of control points) in problems with incomplete Dirichlet boundaries.

5. RESULTS AND DISCUSSION

In this section the effect of number of Lagrange multipliers (N_l) on accuracy of proposed method is investigated for all numerical examples. The time cost is also compared for different meshing refinements in all three methods. In Figure 20 the effect of N_l on error-norm is shown for all numerical examples ($OF=3$). Some features are similar in all examples. It is observed that in each example all curves have a same trend by meshing improvement. Moreover, more Lagrange multipliers are needed to obtain the minimum error as number of elements increases. In addition to similar features, all of them have a specific trend. In the all problems, increasing N_l reduces the errors rate and the present approach has provided the optimal convergence rate in comparison with the other techniques.

Table 1. Comparing time cost between three methods in all numerical examples

	Number of elements	Time (s)		
		LM	***DM***	***TM***
Potential equation problem	12	21.25	18.52	18.84
	14	35.93	30.46	29.69
	16	54.04	46.34	46.51
	18	71.98	71.23	69.33
	20	104.86	100.85	101.00
Cantilever beam problem	10	15.24	10.88	10.25
	12	21.25	15.02	14.31
	14	28.47	20.16	19.58
	16	38.14	27.28	26.47
	18	49.15	36.25	35.61
	20	60.25	46.99	47.30
Infinite plate problem	10	24.52	14.46	13.93
	20	57.49	52.26	45.19
	30	128.36	107.04	98.32
	40	228.64	191.06	175.86
	50	362.41	323.2	293.14
Hollow disk problem	10	10.99	8.87	9.34
	12	25.32	24.00	24.54
	16	59.54	57.79	58.02
	20	123.09	138.00	122.46

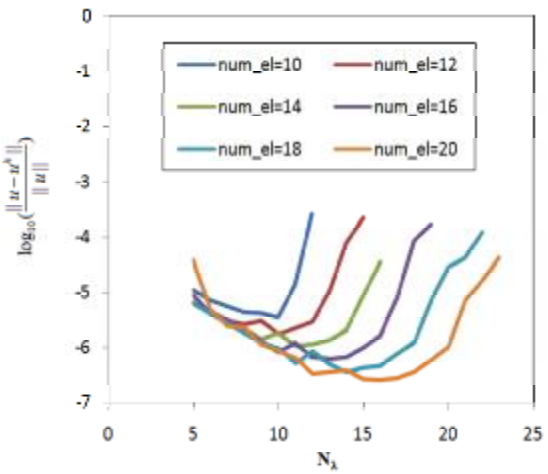

(a) Potential equation

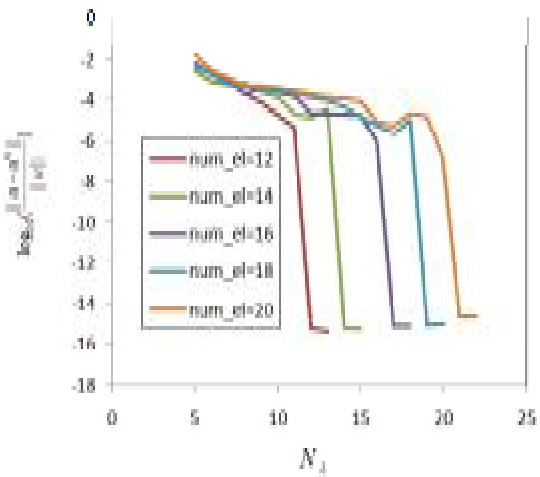

(b) Cantilever beam problem

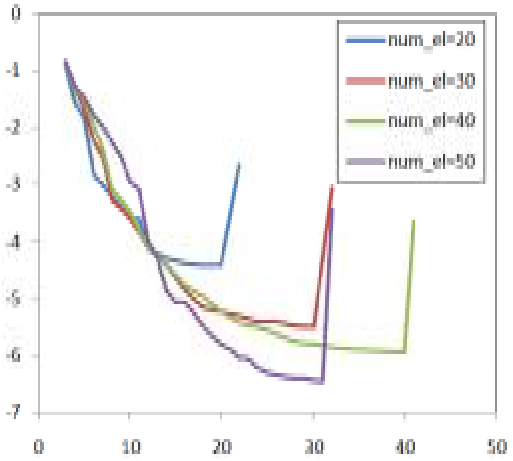

(c) Infinite plate problem

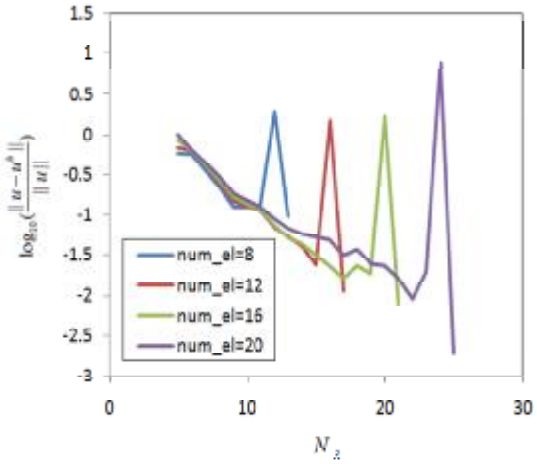

(d) Hollow disk problem

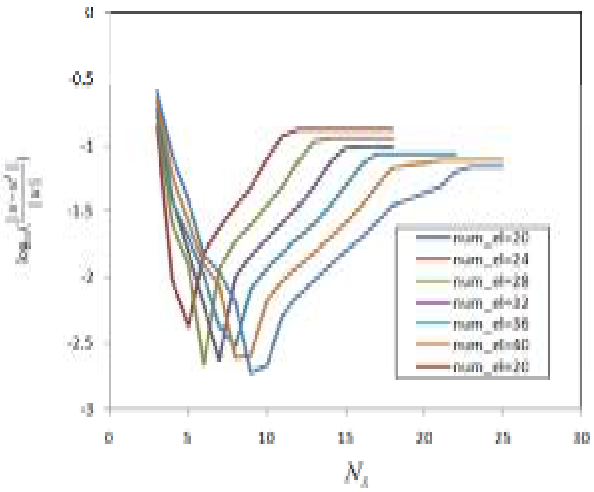

(e) Incomplete Dirichlet boundary

Figure 20. Effect of number of Lagrange multipliers on error-norm in LM

6. CONCLUSION

Lagrange multiplier method is adapted for imposition of essential boundary conditions in isogeomertric analysis. Unlike direct and transformation methods which are based on separation of control points, this method can model incomplete Dirichlet boundaries. The solution accuracy and convergence rates of this method are compared with direct and transformation methods through various numerical examples. The results of numerical examples confirms that the proposed method show more solution accuracy and better convergence rates in comparison with direct and transformation method.

REFERENCES

1. Hughes, TJR, Cottrell JA, Bazilevs Y. Isogeometric analysis: CAD, finite elements, NURBS, exact geometry and mesh refinement. *Comput Meth Appl Mech Eng*, 2005; **194**: 4135–95.
2. Bazilevs Y, Hughes TJR. NURBS-based isogeometric analysis for the computation of flows about rotating components. *Comput Mech*, 2008; **43:** 143–50.
3. Bazilevs Y, Michler C, Calo VM, Hughes TJR. Weak Dirichlet boundary conditions for wall-bounded turbulent flows. *Comput Meth Appl Mech Eng*, 2007; **196**: 4853–62.
4. Bazilevs Y, Calo VM, Hughes TJR, Zhang Y. Isogeometric fluid–structure interaction: theory, algorithms and computations. *Comput Mech*, 2008; **43**: 3–37.
5. Hughes TJR, Reali A, Sangalli G. Duality and unified analysis of discrete approximations in structural dynamics and wave propagation: comparison of p-method finite elements with k-method NURBS. *Comput Meth Appl Mech Eng*, 2008; **197**: 4104–24.
6. Zhang YJ, Bazilevs Y, Goswami S, Bajaj CL, Hughes TJR. Patient-specific vascular NURBS modeling for isogeometric analysis of blood flow. *Comput Meth Appl Mech Eng*, 2007; **196**: 2943–59.
7. Cottrell JA, Reali A, Bazilevs Y, Hughes TJR. Isogeometric analysis of structural vibrations. *Comput Meth Appl Mech Eng*, 2006; **195**: 5257–96.
8. Benson DJ, Bazilevs Y, Hsu MC, Hughes TJR. Isogeometric shell analysis: the Reissner–Mindlin shell. *Comput Meth Appl Mech Eng*, 2010; **199**: 276–89.
9. Gómez H, Calo VM, Bazilevs Y, Hughes TJR. Isogeometric analysis of the Cahn–Hilliard phase-field model. *Comput Meth Appl Mech Eng*, 2008; **197**: 4333–52.
10. Lu J. Circular element: isogeometric elements of smooth boundary. *Comput Meth Appl Mech Eng*, 2009; **198**: 2391–402.
11. Bazilevs Y, Calo VM, Cottrell JA, Evans JA, Hughes TJR, Lipton S, Scott MA, Sederberg TW. Isogeometric analysis using T-splines. *Comput Meth Appl Mech Eng*, 2010; **199**: 229–63.
12. Döfel MR, Jüttler B, Simeon B. Adaptive isogeometric analysis by local h-refinement with T-splines. *Comput Meth Appl Mech Eng*, 2010; **199**: 264–75.
13. Wang D, Xuan J. An improved NURBS-based isogeometric analysis with enhanced treatment of essential boundary conditions, *Comput Meth Appl Mech Eng*, 2010; **199**: 2425-36.
14. Chen JS, Wang HP. New boundary condition treatments in meshless computation of contact problems. *Comput Meth Appl Mech Eng*, 2000; **187**: 441–68.
15. Babuška I. The finite element method with Lagrangian multipliers. *Numer Math*, 1973; **20**: 179-92.
16. Stenberg R. On some techniques for approximating boundary conditions in the finite element method. *J Comput Appl Math*, 1995; **63**: 139–48.
17. Barbosa HJC, Hughes TJR. The finite element method with Lagrange multipliers on the boundary: circumventing the Babuska-Brezzi condition. *Comput Meth Appl Mech Eng*, 1991; **85**: 109–28.
18. Gunzburger MD, Hou SL. Treating inhomogeneous essential boundary conditions in finite element method and the calculation of boundary stresses. *J Numer Anal*, 1992; **29**:

390–24.
19. Moës N, B´echet E, and Tourbier M. Imposing essential boundary conditions in the extended finite element method, *VIII International Conference on Computational Plasticity* 2005.
20. Béchet É, Moës N, Wohlmuth B. A stable Lagrange multiplier space for stiff interface conditions within the extended finite element method. *Int J Numer Meth Eng*, 2009; **78**: 931–54.
21. Leem KH, Oliveira S, Stewart DE. Algebraic multigrid (AMG) for saddle point systems from meshfree discretizations, *Numer Linear Algebra Appl,* 2004; **11**: 293–308.
22. Fernández-Méndez S, Huerta A. Imposing essential boundary conditions in mesh-free methods. *Comput Meth Appl Mech Eng*, 2004; **193**: 1257–75.
23. Belytschko T, Lu YY, Gu L. Element-free Galerkin methods, *Int J Numer Meth Eng,* 1994; **37**: 229–56.
24. Grindeanu I, Kim NH, Choi KK, Chen JS. CAD-based shape optimization using a mesh free method, *Concurrent Eng*, 2002; **10**: 55–66.
25. Cottrell JA, Hughes TJR, Bazilevs Y. Isogeometric analysis (toward integration of CAD and FEA). *1st ed. John Wiley & Sons*. UK, 2009.
26. Piegl L, Tiller W. *The NURBS Book* (Monographs in visual communication), 2nd ed. Springer. New York , 1997.
27. Timoshenko SP, Goodier JN. *Theory of Elasticity*. 3rd ed., McGraw, New York, 1970.